Observer for thick layer of solid Deuterium-Tritium using backlit optical shadowgraphy and interferometry

Alexandre Choux[★✠], Eric Busvelle[✠], Jean Paul Gauthier[✠], Ghislain Pascal[★]
[★]CEA Valduc, DRMN/SMCI/L2C,
21 120 Is sur Tille, France
[✠]Université de Bourgogne, Le2i, UMR CNRS 5158,
9 avenue Alain Savary, 21 000 Dijon, France
alexandre.choux@cea.fr, alexandre.choux@caramail.com
busvelle@u_bourgogne.fr
gauthier@u_bourgogne.fr
ghislain.pascal@cea.fr

December 11, 2006

Abstract

In this paper we present a new method for three dimensional reconstruction from incomplete data-set on a cryogenic hydrogen-isotopes layer.

On the shadowgraphic image, we observe bright rings, that are intersections between caustics and the CCD sensor. Caustics contain informations on the inner cryogenic-layer surface but also on its tangent plane. From the bright ring deformation, we can reconstruct the 3D perturbation along a curve on the considered surface.

Combining interferometric measurements with the shadowgraphic data, an algorithm for the 3D estimation of the inner-surface perturbation is designed. The final reconstruction is based upon a combination of spherical harmonics.

Keywords : cryogenic microshells, shadowgraphy, caustics, data reconciliation, 3D reconstruction.

1 INTRODUCTION

The Laser-Mégajoule project (LMJ) is the french project on inertial confinement fusion [1]. The thermonuclear fusion or ignition shall be obtained by the implosion of solid deuterium-tritium (DT) fuel layer inside a plastic spherical shell. This cryogenic target is a 100 μm thick layer of solid deuterium-tritium at 18.2K uniformly distributed around the inner surface of a 175 μm thick spherical polymer shell with diameter 2430 μm. This one is located at the center of a cylindrical hollow cavity.

The ice layer is approximately conformed by natural self heating due to the radioactive decay to tritium, called β-layering. The DT sublimates from the thicker parts of the layer and recrystallizes and deposits on the thinner parts of the layer. More details about the β-layering process can found in [2] and [3]. The final conformation of the DT-layer will be optimized by precise control of the thermal environment of the shell.

In order to achieve ignition by inertial confinement fusion, the physicist's requirements, that are due to theoretical modeling, for DT-layer thickness and "roughness"[1] are extremely stringent (on shadowgraphic images, the "roughness" must be less than 1 μm [4] and the accuracy on the thickness less than 1 μm). If the DT layer is perturbed by any thermal effect, or if the roughness is too important, some hydrodynamics instabilities could happen during the implosion. This target will be positioned to be shot by the laser only when the specification of the roughness and the homogeneity of the layer will be obtained. For these reason, the DT-ice quality has to be known precisely.

The DT-layer can be observed only through a pair of laser entry holes in the lateral faces of the cylindrical cavity. This is the major constraint that restricts the possibility to get informations on the thickness of the solid DT layer.

Therefore backlit optical shadowgraphy is relevant to measure the DT inner surface along an equator d located in a plane perpendicular to the optical axis.

Other measurements are obtained by interferometry [5] (optical coherent tomography) and provide direct measures of the thickness of the DT-layer in

[1]The "roughness" along an equator is, following the CEA, the square root of the energy of harmonics of order ≥ 2.

two small regions along the optical axis (called the poles here in).

However, up to now in practice, we have only the shadowgraphic measurements. Here in, the interferometric measurements come from simulations.

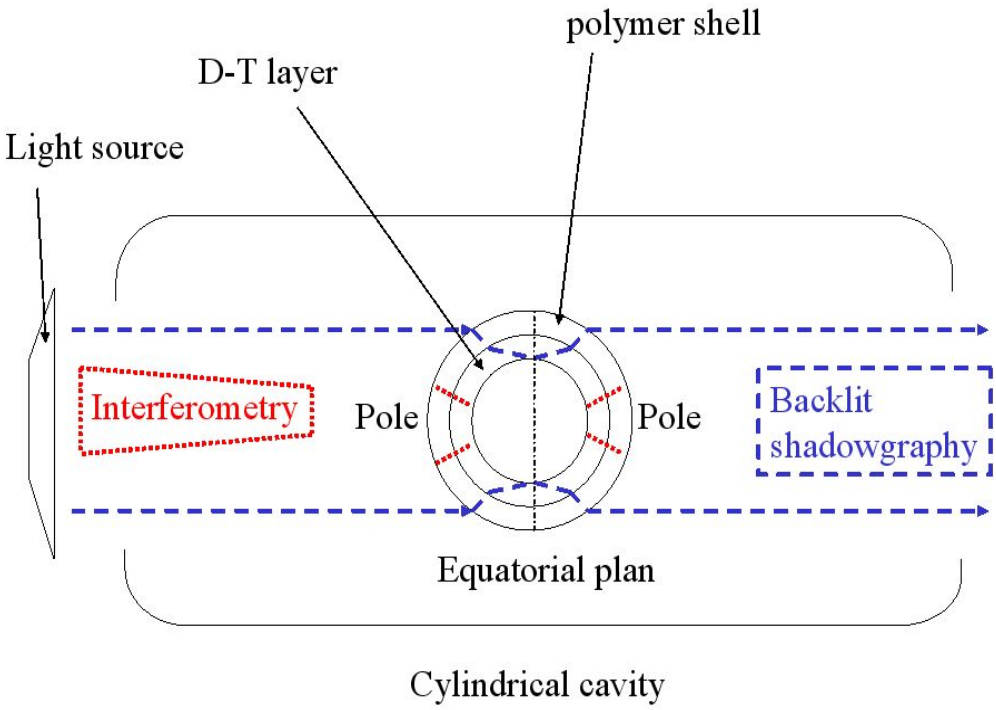

Figure 1: Different methods to obtain information on the cryogenic layer

The content of the paper is as follows:

- First of all, the principle of the backlit optical shadowgraphy will be recalled in the case of our system. We will notice the appearance of a series of bright rings (**caustics**) corresponding to several types of optical paths. In the paper, we will focus on the main bright ring only. We will show how to establish the equation of this ring in the ideal case of a perfectly spherical and centered DT-layer.

- The ideal bright ring is subject to certain perturbations that we assume to be small. The detection of the perturbed bright ring and its analysis will be detailed.

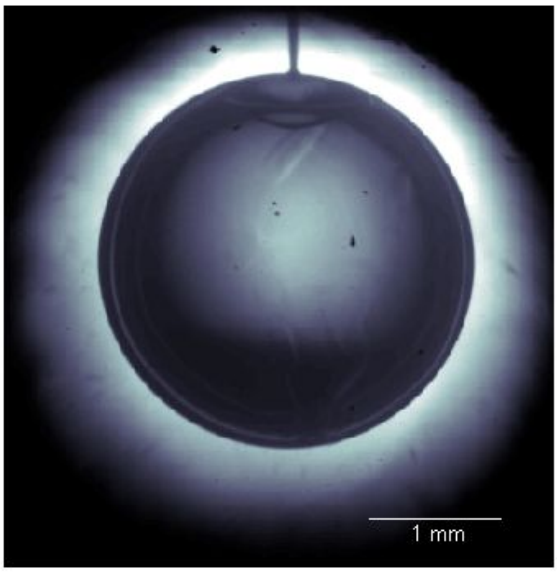

Figure 2: Shadowgraphic picture of a cryogenic layer in an experimental cryostat

- There is a link between these perturbations and the perturbations of the inner surface of the DT-layer. The main fact is that, as caustics, the rings give informations not only on the shape of the inner surface, but **also on its tangent plane**. Linearized formulas of this link will be stated.
- At the end, we will conciliate two types of informations: 1) the informations along the equator, of the perturbations of the DT-layer and the perturbation of its tangent plane, and 2) the direct interferometric measurements at the pole. We will therefore obtain, by certain interpolation–approximation procedure, a final expansion of the inner surface of the DT-layer in terms of spherical harmonics.

2 SHADOWGRAPHY AND IDEAL CAUS-

TIC

The backlit optical shadowgraphy is a technique which consists of putting the studied object between a light source and a camera. The collimated light comes from a source and goes across the cavity before the camera. The pictures that are obtained show the shadow of the lighted object, as we can see on the Figure 2. Due to permeability to light, with different refraction indices, of both the spherical shell and the DT-layer, a single light ray from the source gives rise to several optical paths, of different energy. Then the final light rays intersect the sensor of the camera (which is located after some optical device) and we get the images.

The studied object is a hydrocarbon polymer microshell (with refractive index of 1.54) that contains a solid layer of Deuterium-Tritium (with refractive index of 1.16). The distance between the center of the microshell and the lens of the camera is twice the focal of the lens, denoted by f ($f = 197.5mm$). The device has an axial symmetry (an optical axis). The camera can be considered as the couple of a lens and a plane-optical-sensor (perpendicular to the optical axis) with 1964*2048 pixels. The size of the pixels is $6 * 6\,\mu$m. The numerical aperture of the lens is 0.084 and the magnitude we get is -3. To observe the shadowgraphic pictures, the light source is a lamp with green-filtered monochromatic spectrum that has no effect on the temperature distribution of the target.

Figure 3 shows the optical paths that will be considered in the shadowgraphy system: light rays go from the left to the right. The rays on the right of Figure 3, after crossing the optical system (a lens) determine a caustic (their envelope). The intersection of this caustic with the sensor plane is the bright ring on Figure 2.

As explained before, we exploit only the main ring, i.e. the one with maximum energy. The corresponding ideal caustic is a perfect circle due to the cylindrical symmetry of the system around the optical axis.

Let us now give the form of the parametric equation of the **ideal caustic**. Due to the cylindrical symmetry, calculations can be done in any plane containing the optical axis (all optical paths stay in such planes).

Let the sensor plane be located at a distance equal to $4f + u$ from the centre of the microshell.

Let $\rho \longrightarrow R_u^*(\rho)$ be the map which to a ray from the left (at distance ρ of the optical axis) associates the distance to the optical axis of the intersection of the corresponding ray on the right (after the lens) with the plane of the sensor.

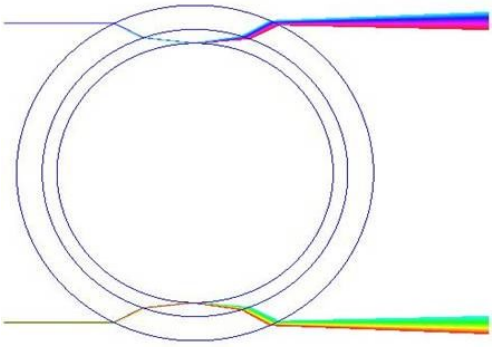

Figure 3: The optical pathes of interest

This map has the following form:

$$R_u^*(\rho) = h_1(\rho) + u\, h_2(\rho),$$

were $h_1(\rho)$ and $h_2(\rho)$ are smooth functions with respect to the variable ρ, depending on the optical system only. They are calculated as a composition of several maps corresponding to the different refraction and reflection steps of the path under consideration, and are given by:

$$h_1(\rho) = \frac{\rho}{\cos 2\Psi} \tag{1}$$

$$h_2(\rho) = \frac{1}{f} h_1(\rho) + \tan 2\Psi \tag{2}$$

with,

$$\begin{aligned}\Psi = \arcsin\frac{\rho}{r_{ext}} - \arcsin\frac{n_{ext}\rho}{n_{\mu b} r_{ext}} + \arcsin\frac{n_{ext}\rho}{n_{\mu b} r_{int}} \\ - \arcsin\frac{n_{ext}\rho}{n_{DT} r_{int}} + \arcsin\frac{n_{ext}\rho}{n_{DT} r_{DT}}\end{aligned} \tag{3}$$

where n_{ext}, $n_{\mu b}$ and n_{DT} are respectively optical indices of exterior environment, microshell and DT; r_{ext} and r_{int} are external and internal radius of the microshell, and r_{DT} is the radius of the DT-layer.

Then, the intersection of the caustic in the u-plane has equation:

$$\frac{\partial R_u^*}{\partial \rho} = 0. \tag{4}$$

In fact, this equation comes from the Jacobian of the ray-tracing map, which is a map from $\mathbb{R}^3$ to $\mathbb{R}^3$. It reduces to this simple equation due to symmetry and to the parametrization (See [6]).

For our fixed ideal u (equals to zero in practice), we get the solution ρ^* of equation 4, determining the ray on the left, such that the corresponding ray on the right intersects the u-plane exactly on the (ideal) caustic.

Then, the radius of the (ideal) bright ring in the u-plane is ($u = 0$)

$$R_c = h_1(\rho^*)$$

Since we consider a single type of optical path, the energy of each ray is the same. Hence we can compute, (by numerical simulation), an irradiance map, giving the ideal lighting of the plane-optical-sensor. Along a radial ray in the sensor plane, we get an intensity profile. The following fact holds:

Fact F: The position of the intersection of the caustic with the sensor plane corresponds to a jump of intensity. Since we are in the case of the simplest stable caustic, this fact will still be true in the perturbed case and exploited for practical detection of the caustic.

3 BRIGHT RING ANALYSIS

We have to perform some image analysis: from the picture in the sensor-plane, we have to reconstruct the main caustic. The purpose of this reconstruction is twofold.

- First, with the results of the next paragraph, using the caustic, we will reconstruct precise information about the inner surface of the DT-layer and its tangent plane on a circle close to the equator plane.

- Second, the physicists define the 2D–roughness (in the equatorial plane perpendicular to the optical axis) as follows. Let $r(\theta)$ be the polar equation of the intersection of the inner surface of the DT-layer with the equator plane.

  The **2D–roughness** is defined as the fraction of the power spectral density of the Fourier decomposition of $r(\theta)$ corresponding to high harmonics.

  Intuitively, as a first approximation, this $r(\theta)$ is proportional to the polar equation of the main caustic. Therefore, having reconstructed

the main caustic, we can perform standard Fourier analysis to compute some approximation of the 2D–roughness.

Due to the **Fact F** above, standard zero-crossing technique can be used to detect precisely the caustic (at the end, with these standard techniques, we will reach the accuracy of 0.1 pixel approximately). We used the very classical method of [9], because of its invariance with respect to 2D–rotations-translations, which is very important in our case, due to the global character of the problem.

Starting from the outer board of the microshell, we encounter a certain number of zeros of the laplacian: the first one corresponds to the shell, the second one to the outer smooth board of the concentration of rays close to the caustic, the third one corresponds to the vertical jump of the caustic, the other zeros correspond to other caustics from different optical paths. Hence we have to detect the third zero crossing.

This one is determined by taking a pixel with positive value and another with negative value around the zero on the profile. Thereby the zero is defined as the weighted barycentre of these two pixels. Using an algorithm following the zeros in the neighborhood of a starting point, the caustic-shape is extracted.

This set of points is unfolded in polar coordinates. Thereafter the points are approximated–interpolated with C^2–splines on the circle using the least square method (it happens that there are large holes on the bright ring, presumably due to non–C^1 perturbations of the surface).

The resulting approximation will be used in the next sections for the global reconstruction of the inner shape of the DT-layer. Moreover, Fourier analysis of this approximation provides the 2D–roughness.

This analysis method has been compared to another one, developed at University of Rochester (see [12]). The results are very similar.

Figure 4 shows a picture from the sensor plane, with a very visible main bright ring.

Figure 5 shows a radial profile corresponding to the red line on the figure 4.

Figure 6 shows the superposition of the reconstructed caustic (its intersection with the sensor plane) and the image.

4 SHADOWGRAPHIC ANALYSIS

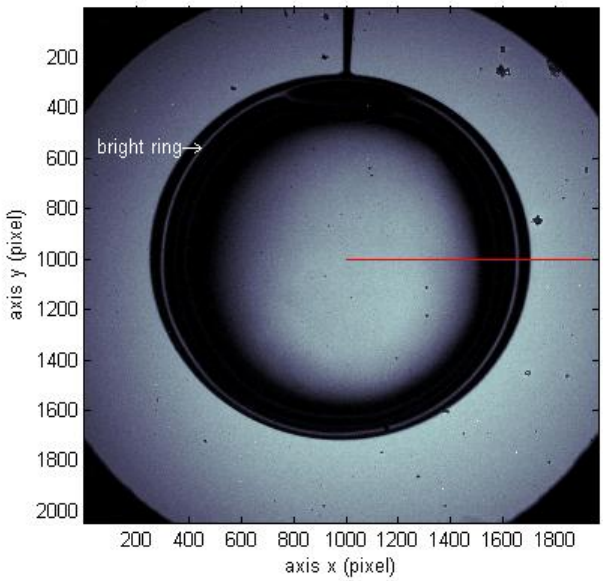

Figure 4: A visible first bright ring

In this section, which contains our most important theoretical results, **we give only the main ideas of computations and proofs**. Detailed proofs and further explanations are given in the Ph.D. thesis [6].

The solid DT layer will always get perturbations on the inner surface, thus the main bright ring will be disturbed. Disturbances on the inner surface can be modelled by a perturbation ε_1 on the radius of the inner sphere, a perturbation ε_2 on the normal vector in the plane (P) determined by the point and the optical axis, and another ε_3 in the perpendicular plane to the previous. In fact, ε_2 is the component (in a natural moving orthonormal frame) of the perturbation, in the direction which is parallel to the tangent of our surface in the direction determined by (P). At first order, it is the same as a (natural) angle between the ideal normal and its perturbation. These perturbations are assumed to be smooth and small in the C^1 sense.

In the following, the notation O^i refers to expressions of order i in ε_1 ,ε_2 ,ε_3 and their first derivatives.

Remark 1 *Note that these three perturbations are not independent. This fact has no consequence in the theoretical results in this section. But, it will be implicitly taken into account when we will merge the whole data by a*

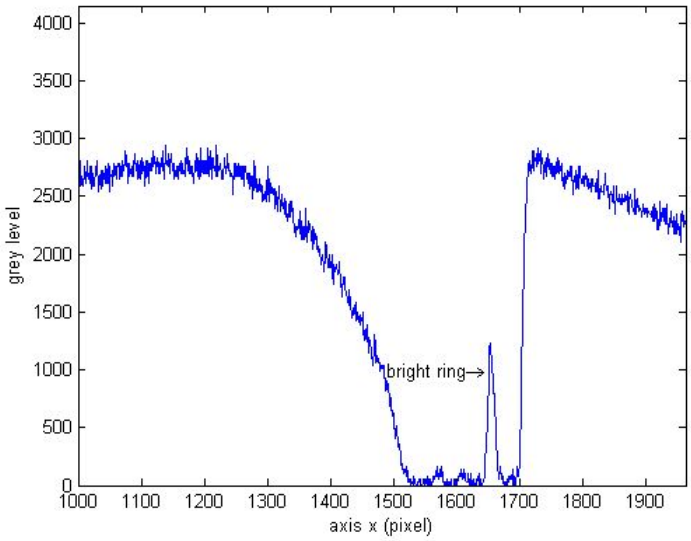

Figure 5: A radial profile

least square method. Since the ε_i's are not independent, these C^1 assumptions correspond to ***the assumption of a small C^2 perturbation of the inner surface of the DT-layer***. *Hence, ε_1 has in fact to be assumed C^2 small for ε_2, ε_3 be C^1 small.*

Let $\rho \in \mathbb{R}$ and $\theta \in [0, 2\pi[$ be the polar coordinates of the starting collimated light ray in a plane perpendicular to the optical axis.

Let $R \in \mathbb{R}$ and $\alpha \in [0, 2\pi[$ be the polar coordinates of the light ray crossing the optical sensor (in its own plane).

Let $R^*(\rho)$ denote the distance to the origin of the intersection point of a ray (starting with coordinate ρ) with the sensor-plane, in the ideal unperturbed situation.

The following theorem is a consequence of both the axial symmetry of the ideal situation and the required smoothness of the perturbation. The proof is just writing explicitly the expansion of the successive refractions and reflections. It is a straightforward but tedious computation. It has been checked by using Mathematica.

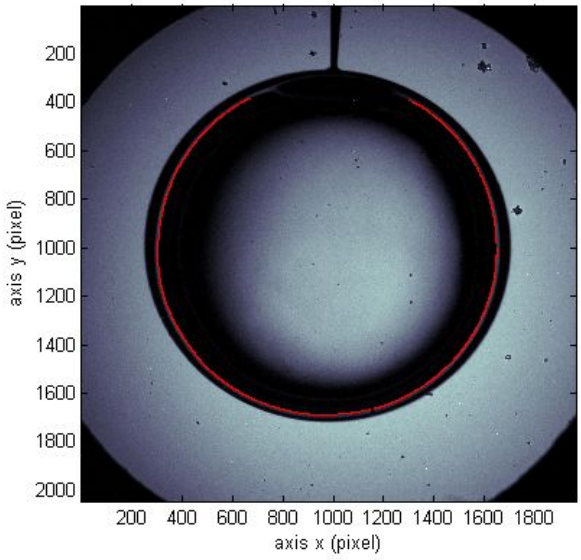

Figure 6: Superposition of the detected caustic.

Theorem 2

$$R(\rho,\theta) = R^*(\rho) + a_1(\rho)\varepsilon_1(\rho,\theta) + a_2(\rho)\varepsilon_2(\rho,\theta) + O^2, \tag{5}$$
$$\alpha(\rho,\theta) = \theta + a_3(\rho)\varepsilon_3(\rho,\theta) + O^2, \tag{6}$$

for certain smooth real functions a_1,a_2,a_3.

Note that the functions a_1, a_2, a_3 depend only on the properties of the optical system.

For the same reasons (symmetry of the ideal situation, and smoothness of the perturbations), the following theorem is easily proved:

Theorem 3 *The equation of the caustic is*

$$\frac{\partial R}{\partial \rho} = 0.$$

A standard fixed point argument shows that we can solve equation (6) in order to get:

$$\theta(\rho,\alpha) = \alpha - a_3(\rho)\varepsilon_3(\rho,\alpha) + O^2. \tag{7}$$

Then replacing (7) in (5) gives:

Theorem 4 *The equation of R in the coordinates (ρ, α) is:*

$$R(\rho, \alpha) = R^*(\rho) + a_1(\rho)\varepsilon_1(\rho, \alpha) + a_2(\rho)\varepsilon_2(\rho, \alpha) + O^2, \tag{8}$$

and the equation of the caustic is still given by $\dfrac{\partial R}{\partial \rho} = 0$ in these coordinates.

Remark 5 *Let us point out that:*

1) computations to obtain the three previous theorems are not obvious,

2) for the proofs of theorem 4, ***the fact that we are on a point of a caustic is crucial.***

3) the perturbation ε_3 has no effect at order 1 on the radius of the caustic.

Now, using the expansion (8) of Theorem 4, we will compute the first order expansion of the caustic of the perturbed system. Let ρ^* denote the radial coordinate of the starting rays of the unperturbed system, intersecting the sensor plane on the ideal caustic. Let φ^* denote the corresponding angle between the ideal ray [from the center of the microshell to the DT-layer] and the optical axis.

Theorem 6 *The equation at order 1 of the perturbed caustic, in the coordinates (ρ, α) is given by:*

$$R_c(\alpha) = R^*(\rho^*) + a_1(\rho^*)\varepsilon_1(\rho^*, \alpha) + a_2(\rho^*)\varepsilon_2(\rho^*, \alpha) + O^2. \tag{9}$$

Proof. The proof again uses deeply the fact that we deal with a caustic. Let us use Theorem 4. If $R_c(\alpha)$ denotes the radius in the sensor plane of the point of the caustic, of angle α, we get, if $\rho^* + \delta\rho$ is the radial value of ρ for the point of the inner DT-layer corresponding to the perturbed caustic:

$$\begin{aligned} 0 = {} & \frac{\partial R^*}{\partial \rho}(\rho^* + \delta\rho) + \frac{\partial a_1}{\partial \rho}(\rho^* + \delta\rho)\varepsilon_1(\rho^* + \delta\rho, \alpha) + a_1(\rho^* + \delta\rho)\frac{\partial \varepsilon_1}{\partial \rho}(\rho^* + \delta\rho, \alpha) \\ & + \frac{\partial a_2}{\partial \rho}(\rho^* + \delta\rho)\varepsilon_2(\rho^* + \delta\rho, \alpha) + a_2(\rho^* + \delta\rho)\frac{\partial \varepsilon_2}{\partial \rho}(\rho^* + \delta\rho, \alpha) + O^2. \end{aligned}$$

Expanding, and using the fact that ε_1 is C^2 small and ε_2 is C^1 small, we obtain:

$$\begin{aligned} 0 = {} & \frac{\partial R^*}{\partial \rho}(\rho^*) + \delta\rho\frac{\partial^2 R^*}{\partial \rho^2}(\rho^*) + \frac{\partial a_1}{\partial \rho}(\rho^*)\varepsilon_1(\rho^*, \alpha) + a_1(\rho^*)\frac{\partial \varepsilon_1}{\partial \rho}(\rho^*, \alpha) \\ & + \frac{\partial a_2}{\partial \rho}(\rho^*)\varepsilon_2(\rho^*, \alpha) + a_2(\rho^*)\frac{\partial \varepsilon_2}{\partial \rho}(\rho^*, \alpha) + \delta\rho O^1 + O^2. \end{aligned}$$

Now, by definition of R^* and ρ^*, and by the fact that the ideal caustic is also characterized by $\frac{\partial R^*}{\partial \rho} = 0$, we have in fact $\frac{\partial R^*}{\partial \rho}(\rho^*) = 0$. Also, straightforward direct computations in the ideal situation show that $\frac{\partial^2 R^*}{\partial \rho^2}(\rho^*)$ is a nonzero constant. From this, we get (using the implicit function theorem) that $\delta\rho = O^1$. Replacing this relation in (8) gives:

$$R_c(\alpha) = R^*(\rho^*+O^1)+a_1(\rho^*+O^1)\varepsilon_1(\rho^*+O^1,\alpha)+a_2(\rho^*+O^1)\varepsilon_2(\rho^*+O^1,\alpha)+O^2,$$

which, at first order gives, using again that $\varepsilon_1, \varepsilon_2$ are C^1 small:

$$R_c(\alpha) = R^*(\rho^*) + \frac{\partial R^*}{\partial \rho}(\rho^*)O^1 + a_1(\rho^*)\varepsilon_1(\rho^*,\alpha) + a_2(\rho^*)\varepsilon_2(\rho^*,\alpha) + O^2.$$

Since, because of the characterization of the ideal caustic, $\frac{\partial R^*}{\partial \rho}(\rho^*) = 0$, we get the result of the theorem. ■

This (affine at order 1) relation (9), using practical measurements of $R_c(\alpha)$ from Section 3 (in which the angle coordinate is α -the angle of a point of the caustic in the sensor plane- **this is very important**), will allow us to recover, by a method explained in the next section, the whole information about the disturbances $\varepsilon_1(\rho^*,\alpha)$ and $\varepsilon_2(\rho^*,\alpha)$ of the ideal spherical surface.

It is also not so hard to prove that (since ε_1 is assumed C^2 small):

$$\varepsilon_3(\rho^*,\theta) = \frac{1}{R\cos^2(\varphi^*)}\frac{\partial \varepsilon_1(\varphi^*,\theta)}{\partial \theta} + O^2. \tag{10}$$

Remark 7 ***(Important)*** *Due to the relations (7, 10), if we know $\varepsilon_1(\rho^*,\alpha)$, it is possible to reconstruct $\theta(\rho^*,\alpha)$ at order 1 in terms of α (which is the angle observed in practice). In fact, it seems that this order 1 correction of the relation at order zero:*

$$\theta(\rho^*,\alpha) = \alpha + O^1, \tag{11}$$

is of no significant importance on the final results. Therefore, in the next section, for the purpose of practical reconstruction of the inner surface of the DT-layer, we will use only relation (11) in place of (10).

5 DT LAYER ESTIMATION

Let us consider the previous angle θ and complete it with the other angle φ, in order to form Euler-like coordinates around the center of the microshell. Then, the inner surface of the DT-layer is modelled as a perturbation $\varepsilon(\theta,\varphi)$

of the ideal spherical inner surface of the DT-layer. As we said above, this perturbation is assumed to be C^2-small. It will be modelled a-priori as a finite sum of spherical harmonics

$$\varepsilon(\theta,\varphi) = \sum\nolimits_{i=1}^{i=k} \lambda_i . e_i(\theta,\varphi). \tag{12}$$

where λ_i are constants and represent the magnitudes of each spherical harmonics $e_i(\theta,\varphi)$.

This is standard: disturbances of spheres are generally modelled by spherical harmonics [7], [8]. **What is not standard here is our choice of the relevant spherical harmonics** $e_i(\theta,\varphi)$. Here, we introduce **some a-priori information**. Practically, we consider only spherical harmonics that can occur in the physical configuration. Main perturbations have mainly three origins: 1) the gravity (the optical axis is in practise vertical), 2) the thermal disturbances coming from the two windows of the cylindrical cavity, that are situated above and below the device, and 3) position errors of the centre of the microshell w.r.t. the centre of the cylindrical cavity. Therefore, we will only keep spherical harmonics that give rise to these perturbations.

Remark 8 ***(Important)*** *Note that this C^2-small disturbance $\varepsilon(\theta,\varphi)$ completely determines our perturbations $\varepsilon_1, \varepsilon_2, \varepsilon_3$ above.*

At this point, our procedure for reconstructing the inner surface of the DT-layer $R + \varepsilon(\theta,\varphi)$ is performed in two different steps:

- First, we will reconstruct $\varepsilon_1(\rho^*,\theta), \varepsilon_2(\rho^*,\theta)$, (and eventually $\varepsilon_3(\rho^*,\theta)$, but, as we said above, this looks unnecessary, the approximation $\theta = \alpha$ from relations (10, 11) being sufficient in practice).

  Equivalently, we reconstruct $\varepsilon_1(\rho^*,\alpha)$, $\varepsilon_2(\rho^*,\alpha)$, $\varepsilon_3(\rho^*,\alpha)$, **that is we reconstruct 1) the intersection of the perturbed inner surface of the DT-layer with the plane corresponding to** ρ^*, **perpendicular to the optical axis, 2) the tangent planes to the inner surface along this curve. This is 3D information (our main contribution).**

- Second, we will reconcile this information with the information obtained at the poles, by direct interferometry measurements.

Both steps are achieved by standard least square procedures.

- In the first step, the a-priori expansion (12) is used in restriction to (the plane) $\{\varphi = \varphi^*\}$: $\varepsilon(\theta,\varphi^*) = \sum\nolimits_{i=1}^{i=k} \lambda_i . e_i(\theta,\varphi^*)$. As we said, we confuse this

relation with the relation $\varepsilon(\alpha, \varphi^*) = \sum_{i=1}^{i=k} \lambda_i . e_i(\alpha, \varphi^*)$. Then, the practical measurements are the values $R_c(\alpha)$, that are considered equal to $R_c(\theta)$, and the main equation:

$$R_c(\alpha) \approx R^*(\rho^*) + a_1(\rho^*)\varepsilon_1(\rho^*, \alpha) + a_2(\rho^*)\varepsilon_2(\rho^*, \alpha),$$

from Theorem 6 gives rise to a set of linear equations, with unknown's the λ_i's, $i = 1, ..., k$.

The number of equations is the number of values of α taken into account. The corresponding values $R_c(\alpha)$ come from the method , described in section 3, to compute the inner part of the bright ring, corresponding to the caustic.

This overdimensioned system of linear equations is solved in the least-squares sense, and provides the curve [on the inner DT-layer, associated with the rays that intersect the caustic in the sensor plane] and the tangent plane to the inner surface along this curve.

-After that, we use this first information together with the direct measurements at the poles, and we reconcile both sets of data via a second standard least-squares step.

To finish, we show now some results of the full 3D Reconstruction of the inner surface of the DT-layer. Up to now, contrarily to the results of Section 3 for the detection of the caustic, these are only simulation results, since we don't have yet the interferometric measurements at the poles.

The figure 7 shows a reconstructed inner surface of the DT-layer. For the same reconstruction, figure 8 shows the real surface compared to the reconstructed surface, along a horizontal and a vertical cut. These deformations are not realistic but have been highlighted on the figures.

6 CONCLUSION

To study the solid DT layer in a hollow cavity along some axial symmetry, backlit optical shadowgraphy seems to be a relevant measurement method. The shadowgraphic images show bright rings that are due to caustics. The detection of the main bright ring provides some 3D information (tangent planes along a certain closed curve close to the equator perpendicular to the optical axis).

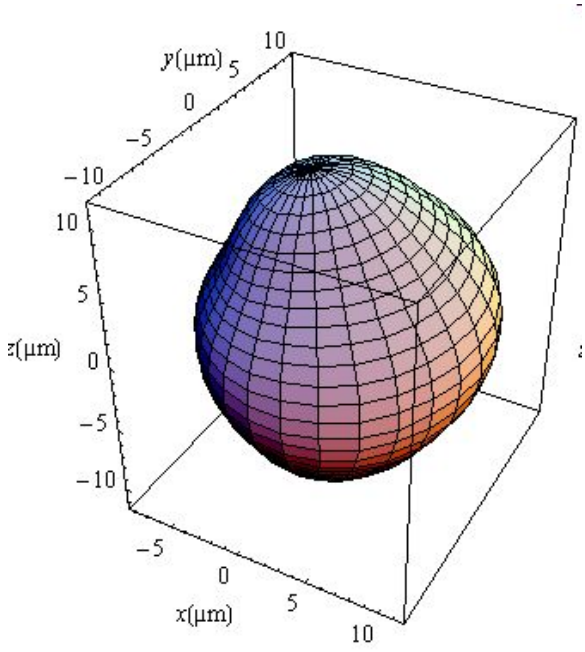

Figure 7: A reconstructed deformation

Because of our main theorem 6, the calculations remain rather reasonable: calculations may be performed assuming that the optical path entirely remains in a plane through the optical axis. These calculations link the distortion of the bright ring to the perturbation of the inner DT layer surface.

From this relation and the detection of the bright ring, the 3D perturbation is partially estimated. Other optical measurements (interferometry) provide direct informations along the poles. A standard method (least-squares on a representation by spherical harmonics), has been developed in order to merge these direct informations with those from the shadowgraphy analysis.

It would be interesting, (and this is certainly possible, since some of them have non negligible energy) to use also the **caustics corresponding to other optical paths**. The main difficulty is that these paths (contrarily to the one we analyzed) correspond to more than a single reflection on the inner DT surface, and therefore will provide mixed information between tangent planes at certain points.

We gratefully acknowledge Pr. V. Zakalyukin, from the Lomonosov Moscow State University, for his intuition of Theorem 6, which is really crucial, since it makes the computations possible in practice.

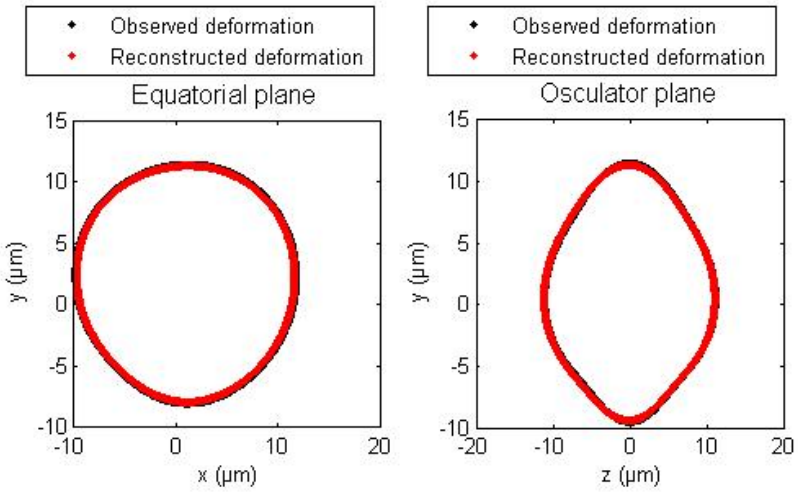

Figure 8: Comparison between cuts of original and reconstructed surfaces.

References

[1] J. D. Lindl, *Inertial Confinement Fusion*, (Springer, 1998).

[2] J. K. Hoffer, L. R. Foreman, "Radioactively Induced Sublimation in Solid Tritium", Physical Review Letters **60**, 1310-1313 (1988).

[3] M. Martin, C. Gauvin, A. Choux, P. Baclet, G. Pascal, "The Cryogenic Target for Ignition on the LMJ: Useful Tools to Achieve Nominal Temperature and Roughness Conditions of the DT Solid Layer", Fusion Science and Technology, **49** n°4, 600-607 (May 2006).

[4] S. Haan and al, "Update on Specifications for NIF Ignition Targets, and Their Rollup into an Error Budget", Fusion Science and Technology, **49** n°4, 553-557 (May 2006).

[5] F. Gillot, A. Choux, L. Jeannot, G. Pascal, P. Baclet, "Characterization of the DT layer of ICF targets by optical techniques", Fusion Science and Technology, **49** n°4, 626-634 (May 2006).

[6] A. Choux, "Commande optimale d'un système de conformation cryogénique d'une couche solide d'isotopes de l'hydrogène dans un microballon par chauffage infra rouge", PhD thesis from University of Burgundy, to be defended December 2006.

[7] E.W. Hobson, *The theory of spherical and ellipsoidal harmonics*, (New York : Chelsea, 1955).

[8] H. Groemer, *Geometric applications of Fourier series and spherical harmonics*, (Cambridge University Press, 1996).

[9] Marr, D. and Hildreth, E. "Theory of edge detection", Proc. R. Soc. Lond. B, **207**, 187-217 (1980).

[10] V. Zakalyukin, "Applications of flag contact singularities", *New Developments in Singularity theory*, Nato series, Kluwer, 41-70 (2001).

[11] V.I. Arnold, A. Varchenko, and S. Goussein-Zadé. *Singularités des Applications Différentiables. I : Classification des Points Critiques, des Caustiques et des Fronts d'Onde.* (Editions Mir, Moscou, 1986).

[12] D.H. Edgell, W. Seka, R.S. Craxton, L.M. Elasky, D.R. Harding, R.L. Keck, L.D. Lund, and M.D. Wittman, "Characterization of cryogenic direct-drive ICF targets during studies and just prior to shot time", Fusion Science and Technology, **49** n°4, 616-625 (May 2006).

List of Figure Captions

Fig. 1 Different methods to obtain information on the cryogenic layer,

Fig. 2 Shadowgraphic picture of a cryogenic layer in an experimental cryostat

Fig. 3 The optical pathes of interest

Fig. 4 A visible first bright ring

Fig. 5 A radial profile

Fig. 6 Superposition of the detected caustic

Fig. 7 A reconstructed deformation

Fig. 8 Comparison between cuts of original and reconstructed surfaces